

An Overview of the Semi-arid Climate and Environment Research Observatory over the Loess Plateau

HUANG Jianping^{*1} (黄建平), ZHANG Wu¹ (张武), ZUO Jinqing¹ (左金清), BI Jianrong¹ (闭建荣),
SHI Jinsen¹ (史晋森), WANG Xin¹ (王鑫), CHANG Zhoulin¹ (常倬林), HUANG Zhongwei¹ (黄忠伟),
YANG Su¹ (杨溯), ZHANG Beidou¹ (张北斗), WANG Guoyin¹ (王国印), FENG Guanghong¹ (冯广泓),
YUAN Jiuyi¹ (袁九毅), ZHANG Lei¹ (张镭), ZUO Hongchao¹ (左洪超), WANG Shigong¹ (王式功),
FU Congbin^{2,1} (符淙斌), and CHOU Jifan¹ (丑纪范)

¹College of Atmospheric Sciences, Lanzhou University, Lanzhou 730000

²Key Laboratory of Regional Climate-Environment for Temperate East Asia (RCE-TEA),
Institute of Atmospheric Physics, Chinese Academy of Sciences, Beijing 100029

(Received 30 May 2007; revised 26 June 2008)

ABSTRACT

Arid and semi-arid areas comprise about 30% of the earth's surface. Changes in climate and climate variability will likely have a significant impact on these regions. The Loess Plateau over Northwest China is a special semi-arid land surface and part of a dust aerosol source. To improve understanding and capture the direct evidence of the impact of human activity on the semi-arid climate over the Loess Plateau, the Semi-Arid Climate and Environment Observatory of Lanzhou University (SACOL) was established in 2005. SACOL consists of a large set of instruments and focuses on: (1) monitoring of long term tendencies in semi-arid climate changes; (2) monitoring of the aerosol effect on the water cycle; (3) studies of interaction between land surface and the atmosphere; (4) improving the land surface and climate models; and (5) validation of space-borne observations. This paper presents a description of SACOL objectives, measurements, and sampling strategies. Preliminary observation results are also reviewed in this paper.

Key words: cloud, aerosol, land surface, semi-arid, Loess Plateau, SACOL

Citation: Huang, J. P., W. Zhang, J. Q. Zuo, J. R. Bi, J. S. Shi, X. Wang, Z. L. Chang, Z. W. Huang, S. Yang, B. D. Zhang, G. Y. Wang, G. H. Feng, J. Y. Yuan, L. Zhang, H. C. Zuo, S. G. Wang, C. B. Fu, and J. F. Chou, 2008: An overview of the semi-arid climate and environment research observatory over the Loess Plateau. *Adv. Atmos. Sci.*, **25**(6), 906–921, doi: 10.1007/s00376-008-0906-7.

1. Introduction

Water and energy cycles are extremely important in understanding the mechanism of climate and environmental change in China because of the severe shortage of water resources and the rapid increase of population, which lead to a significant anthropological impact on the climate and environment due to land-use and greenhouse gas emissions. Anthropogenic emissions of greenhouse gases cause an increase in surface temperatures (the “greenhouse effect”) and can have profound effects on the climate and thus on societal welfare. Brought on by more than a factor of 5, the

increase in human population and the subsequent activities of mankind over the last century or so, greenhouse gases and aerosols produced by the combustion of fossil fuels, industrial activities, and land use have altered the atmospheric composition so that it is not the same as it was a century ago (Mann et al., 1999; Crowley, 2000; Houghton et al., 2001). The resulting increase in surface temperature over this period is estimated to be between 0.4°C to 0.8°C (Houghton et al., 2001). Aerosol particles also have a major influence on the global climate and climate change; they can locally either intensify or moderate the effects of the greenhouse gases through the scattering or absorp-

*Corresponding author: HUANG Jianping, hjp@lzu.edu.cn

tion of both incoming solar radiation and thermal radiation emitted from Earth's surface. Aerosols also act as cloud condensation nuclei (CCN) and thereby modify the radiative properties of clouds (Twomey, 1977). There is substantial uncertainty regarding the magnitude and spatial distribution of aerosol radiative forcing. Ramanathan et al. (2001) suggested that a combination of the aerosol direct and indirect effect can weaken the hydrological cycle, which could be a major environmental issue in this century.

To better understand and quantify the human-induced climate effect, a variety of global climatic observation networks have been established recently to characterize the physical and chemical properties and processes of greenhouse gases and aerosols. These include the Baseline Surface Radiation Network (BSRN) (<http://bsrn.ethz.ch>), CEOP (Coordinated Enhanced Observing Period) (<http://www.gewex.org/ceop.htm>); AERONET (Aerosol Robotic Network) (Holben et al., 1998); MPLNET (Micro-Pulse Lidar Network) (Welton et al., 2001); and so on. BSRN is a project of the World Climate Research Programme (WCRP) and the Global Energy and Water Experiment (GEWEX) and as such is aimed at detecting important changes in the earth's radiation field at the earth's surface that may be related to climate change. The data are of primary importance in supporting the validation and confirmation of satellite and computer model estimates of these quantities. CEOP was initiated as a major step towards bringing together the research activities in GHP (GEWEX Hydrometeorology Panel)/GEWEX (Global Energy and Water Cycle Experiment) and related projects in WCRP (CLIVAR; CLiC). CEOP has now developed into an important element of WCRP. It has also been endorsed by the Integrated Global Observing Strategy Partnership (IGOS-P) as the first element of the IGOS-P Integrated Global Water Cycle Observations (IGWCO) Theme. As a result of a decision at the 2005 meeting of the WCRP Joint Scientific Committee, the oversight of CEOP is shared between GEWEX and the WCRP Observation and Assimilation Panel (WOAP). BSRN is aimed at detecting important changes in the earth's radiation field at the earth's surface which may be related to climate change; AERONET is a ground-based remote sensing aerosol network that provides a long-term, continuous and readily accessible public domain database of aerosol optical, microphysical and radiative properties for aerosol research and characterization, validation of satellite retrievals, and synergism with other databases (Holben et al., 1998); MPLNET is comprised of ground-based lidar systems, co-located with sun/sky photometer sites in AERONET. The com-

bined lidar and sunphotometer measurements are able to produce quantitative aerosol and cloud products, such as optical depth, sky radiance, vertical structure, and extinction profiles.

Arid and semi-arid areas comprise about 30% of the earth's surface. Changes in climate and climate variability will likely have a significant impact on these regions. Some field experiments have recently been carried out over the arid and semiarid regions of China over the past 30 years, for example HEIFE (Hu, 1994; Hu and Gao, 1994), IMGRASS (Lu et al., 2002, 2005), NWC-ALIEX (Huang, 2004; Zhang et al., 2005; Bao and Lu, 2006), dust aerosol observations in Dunhuang (Iwasaka et al., 2003, 2004), surface layer turbulent flux observations over Naiman (Zhang et al., 2001) and Tongyu (Liu et al., 2004), etc., in which a great deal of observational data and research achievements were gained. However, there was little learned of the Loess Plateau and there was no international long-term observation site for the Loess Plateau. Loess Plateau is the largest arid and semi-arid zone in China and is also one of the dust aerosol sources. To fill this gap and improve understanding of the impact of human activity on semi-arid climate over the Loess Plateau, the Semi-Arid Climate & Environment Observatory of Lanzhou University (SACOL) was established in 2005. This site is nearby the city of Lanzhou, at the southern bank of the Yellow River in northwestern China. In addition, the site is very close to the geometric center of China's mainland. This region includes many types of aerosol particles of widely varying composition and sizes derived from one of the largest aerosol source regions on the earth. SACOL makes several important measurements of wind-blown dust, urban pollution, and radiation properties. SACOL is specifically designed to assess the dust aerosol effect on local climate as well as the global climate. Most of the instruments in SACOL are based at the BSRN, CEOP, AERONET and MPLNET. The main focus of SACOL is on assessing and improving the new data products being derived from these instruments to increase our knowledge and reduce uncertainties associated with atmospheric aerosols and their radiative impacts. SACOL also plays a critical role in testing and improving the satellite algorithms over the Loess Plateau because of the unusually complete datasets that are obtained to characterize properties of the atmosphere and surface. Furthermore, the measurements provide details about aerosols, such as particular height-resolved aerosol radiative and microphysical properties, some of which cannot be retrieved from any current or anticipated satellite data; these data are a test bed for current aerosol and chemical transport models. Details regarding SACOL objectives, platforms, instrumenta-

tion, measurement strategy, and a summary of early results are given below.

2. Scientific objectives

The SACOL site offers attractive opportunities to study certain phenomena that are believed to be important to the drought process. These phenomena form the focus for the SACOL. The primary objective of SACOL is the elucidation of drought processes in such a way that their physical description can be accurately incorporated into global or regional climate models. These models include parameterizations of a variety of physical, chemical, and biological processes occurring in the coupled atmosphere-land surface, that, taken together and working in concert, are designed to simulate and predict the climate system, with all its relevant feedback mechanisms that dominate climate regionally as well as globally.

Recently, special attention has been dedicated to cloud interactions with desert aerosol particles (Rosenfeld et al., 2001; Bréon et al., 2002; DeMott et al., 2003; Kawamoto and Nakajima, 2003; Huang et al., 2006a,b). However, the knowledge of the effects of Asian dust aerosols on arid climate is still very limited due to the lack of observations. Aerosols are generally believed to exert a cooling influence on the climate directly by scattering solar radiation and through their indirect effects on clouds. However, the semi-direct effect has the potential to offset this cooling by reducing low cloud cover and water path. Analysis of the satellite observations indicates that, on average, the water path of dusty clouds is considerably smaller than that from dust-free clouds in the same frontal systems. The key issue may be related to the dust aerosol warming effect through the absorption of solar radiation. The absorption or diabatic heating of Asian dust particles can cause the evaporation of cloud droplets and reduce the cloud water path (Huang et al., 2006a,b). Due to the large spatial and temporal extent of desert dust in the atmosphere, the interactions of desert dust with clouds can have substantial climatic impacts. Dust storms may have contributed to the desertification of Northwest China during recent decades. To better understand the effect of Asian dust on regional climate, one of the important objectives of SACOL is to focus on measurements of physical processes of aerosol-climate interactions.

Satellites, which offer a global perspective with high spatial and temporal resolution, have become important tools for measuring the changing characteristics of the climate system and the associated radiative heat fluxes that define the climate. Improvements in satellite sensor technologies and constituent retrieval

techniques have helped to advance our understanding of the climate system. Hence, improvement of the Loess Plateau satellite remote sensing is a relevant and important scientific objective of the SACOL. The major scientific objectives of SACOL are to monitor long term tendencies in semi-arid climate changes; the aerosol effect on the water cycle; characterize the interaction between the land surface and the atmosphere; form a base for the land surface in climate modeling and validation of space-borne observations.

3. Location and climatology

SACOL is about 48 km away from the center of Lanzhou, situated at the southern bank of the Yellow River in the Gansu province in Northwest China (35.57°N, 104.08°E). It is situated on the China-Loess Plateau, about 1965.8 m above sea level. The topography around the site is characterized by the Loess Plateau consisting of plain, ridge and mound, etc, with the elevation ranging between 1714–2089 m. The parent soil material is mainly quaternary aeolian loess with the main soil type being sierozem. There is also some loess soil in the terrace, ridge and mound. The terrain where the measurements are carried out is flat and covered with short grass. The dominated species within the immediate area are *stipa bungeana* as well as *artemisia frigida* and *leymus secalinus*. Figure 1 shows the typical landscape around the site. Figure 2 shows the map of SACOL's location. The climatological information is listed in Table 1. The annual variations of surface temperature and precipitation are displayed in Fig. 3. A maximum of surface temperature is found in July and a minimum in late winter. However, a maximum of precipitation is observed in August.

Based on the available original dust event records from the Yuzhong meteorological stations, the monthly means of the average observed days with surface spring dust events around the SACOL site are plotted in Fig. 4. Dust events can be classified into three categories depending on the meteorological condition: floating-dust (FD), blowing dust (BD) and dust storm (DS). The overall 45-year (1960–2004) annual mean FD value of 18 days is about 139% greater than the mean BD value of 7.53 days and 1057% greater than mean DS of 1.53 days.

4. Measurements

SACOL was established at the Yuzhong campus of Lanzhou University in late 2005. It consists of a large set of instruments and measure: (1) boundary layer meteorological parameters; (2) surface radiation; (3)



Fig. 1. Multiple views of the SACOL site.



Fig. 2. Map of SACOL's location.

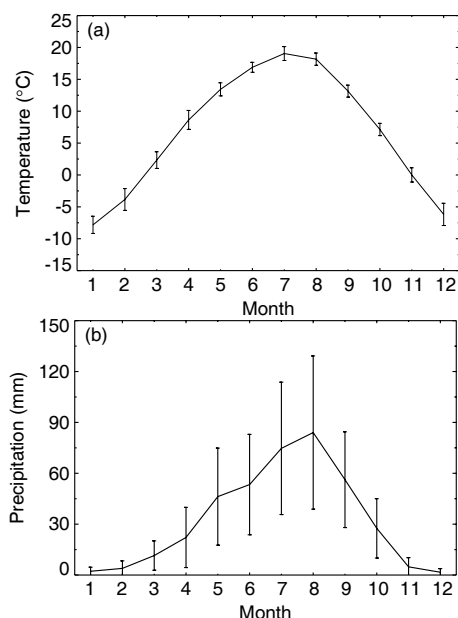


Fig. 3. Monthly mean and standard deviation of meteorological parameters at SACOL for (a) surface temperature; and (b) precipitation.

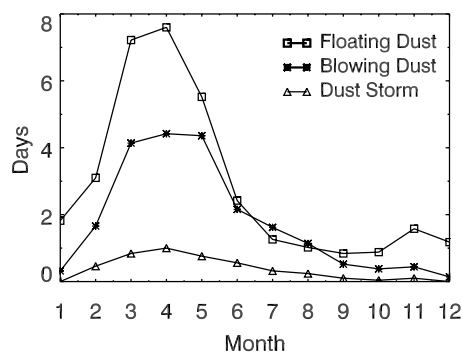


Fig. 4. Monthly variations of dust event at SACOL.

surface fluxes; (4) soil heat and water moisture; (5) ambient air quality; (6) aerosol optical properties; (7) temperature and water vapor profiles; (8) sky conditions. SACOL is a participating site in the Coordinated Enhanced Observing Period (CEOP) which was initiated as a major step towards bringing together the research activities in GHP/GEWEX and related projects in WCRP (CLIVAR; CLiC). CEOP has now developed into an important element of WCRP. It has also been endorsed by the Integrated Global Observing Strategy Partnership (IGOS-P) as the first element of the IGOS-P Integrated Global Water Cycle Observations (IGWCO) Theme. An AERONET-Cimel sun photometer for spectral, radiative, and aerosol optical properties (Holben et al., 1998) has been measured and archived at SACOL. The Micro-Pulse Lidar Network (MPLnet) lidar (Welton et al., 2001) is also operational at SACOL. It provides real-time images of the vertical profile of backscatter. Many additional measurements made at SACOL are shown in Table 2. The details about the instruments are introduced as following:

4.1 Boundary layer meteorological measurements system

Boundary layer meteorological measurements (Fig. 5a) include wind speed (014A-L, Met One), air temperature and relative humidity (HMP45C-L, Vaisalla) at 1, 2, 4, 8, 12, 16 and 32 m, and wind direction (034B-L, Met One) at 8 m, with signals logged to a data logger (CR23X, Campbell) and recorded at half-hour intervals. The measurement of skin temperature is made with a Precision Infrared Thermocouple Sensor (IRTS-P, Apogee). Barometric pressure is measured using a CS105 Barometric Pressure Sensor (Vaisala) over a 600 to 1060 hPa range. Precipitation is measured with a tipping bucket Rain Gage (TE525MM-L, Texas Electronics) in 0.1 mm increments.

Table 1. Surface and climate parameters.

Parameter	Description
Surface Type	Loess tableland, ridge, hillock and gully
Landscape	crop and semi-desert
Climate	continental monsoon zone
Annual precipitation	381.8 mm
Annual mean evaporation	1528.5 mm
Annual mean air temperature	6.7°C
Annual mean highest temperature	13.7°C
Annual mean lowest temperature	0.8°C

Table 2. Instruments and parameters measured from the semi-arid climate and environment of Lanzhou University.

Description	Model	Manufacturer
Wind speed sensor	014A_L	Met One
Wind direction sensor	034B_L	Met One
Humidity and temperature probe	HMP45C-L	Vaisala
Surface temperature sensor	IRTS-P	Apogee
Barometric pressure sensor	CS105	Vaisala
Tipping bucket rain gage	TE525MM-L	R. M Young
Pyranometer (SW flux)	CM21	Kipp & Zonen
Normal incidence pyrhelimeter (DIRECT)	MODEL NIP	Eppley
Pyrhelimeter	CH 1	Kipp & Zonen
UV radiometer (UV-A & UV-B)	UV-S-AB-T	Kipp & Zonen
Pyrgeometer (LW flux)	CG4	Kipp & Zonen
UV-Multi-filter rotating shadow-band radiometer	UVMFR-7	Yankee
Multi-filter rotating shadow-band radiometer	MFR-7	Yankee
3-D Sonic anemometer	CSAT3	Campbell
Opened path infrared CO ₂ & H ₂ O analyzer	LI7500	Li-Cor
Large Aperture Scintillometer	LAS	Kipp & Zonen
Water content reflectometer	CS616-L	Campbell
Soil temperature profile	STP01-L50	Hukseflux
Soil Heat flux plate	HFP01SC-L50	Hukseflux
SO ₂ analyzer	ML9850B	Ecotech
NO/NO ₂ /NO _x analyzer	ML9841B	Ecotech
Ozone analyzer	ML9810B	Ecotech
CO analyzer	ML9830B	Ecotech
PM10 Ambient Particulate Monitor	RP 1400a	R & P
Non Methane Hydrocarbons Analyzer	PCF NMHC 527	PCF
Micro-Pulse Lidar	MPL-4	Sigma Space
CAML TM Micro lidar	CE370-2	Cimel & CNRS
Sun photometer	CE318 (AERONET)	Cimel
Integrating Nephelometer (3-wavelength)	TSI 3563	TSI
Integrating Nephelometer (450, 550, 700 nm)	M9003	Ecotech
Aerodynamic Particle Sizer Spectrometer (0.5 to 20 μm aerodynamic sizing, 0.37 to 20 μm optical detection)	TSI 3321	TSI
Aethalometer (aerosol light absorption)	AE-31	Magee
Dual Band for Temperature, Water Vapor & Liquid Water Profiles	TP/WVP-3000	Radiometrics Corporation
Total Sky Imager	TSI 880	Yankee

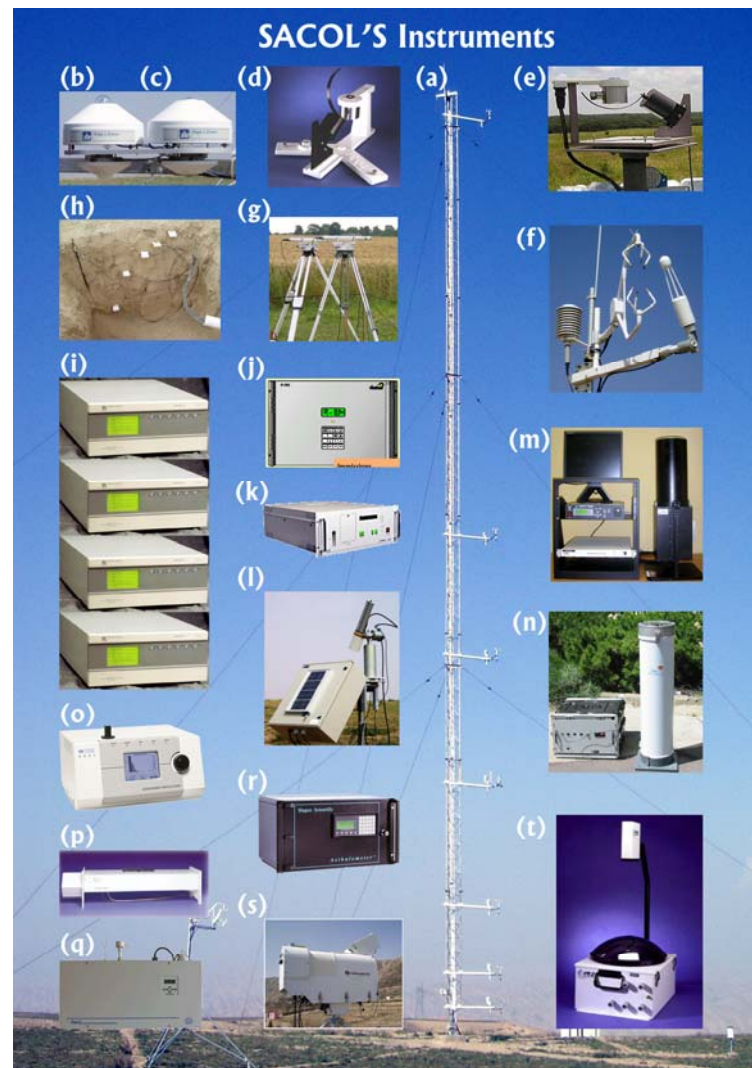


Fig. 5. Instruments for (a) Boundary layer meteorological measurements; (b)–(e) Surface radiation monitoring; (f) and (g) Surface fluxes monitoring; (h) Soil parameters monitoring; (i)–(k) Ambient air analyzers; (l)–(r) Aerosol optical properties measurements; (s) Temperature and water vapor profiles; and (t) Sky conditions measurement.

4.2 Surface radiation monitoring system

The surface radiation monitoring system consists of upward and downward pyranometers (CM21, Kipp & Zonen) (Fig. 5b) for incoming and outgoing short-wave radiation; and upward and downward pygeometers (CG4, Kipp & Zonen) (Fig. 5c) for incoming and outgoing longwave radiation. In addition, spectral measurements of total, diffuse and direct solar irradiances are made with a set of two multi-filter rotating shadow-band radiometers [UVMFR-7 (Fig. 5d) and MFR-7 (Fig. 5e)] with seven channels in the UV (300, 305.5, 311.4, 317.6, 325.4, 332.4 and 368 nm) and the visible (415, 500, 615, 673, 870, and 940 nm), respec-

tively. From those measurements, the properties of clouds (Min, 1996) and the atmosphere (Harrison et al., 1994; Harrison and Michalsky, 1994; Alexandrov et al., 1999) can be derived, such as the column abundances of ozone and water vapor as well as aerosol and other atmospheric constituents.

4.3 Surface fluxes monitoring system

4.3.1 Eddy covariance system

The fluxes of momentum, CO₂, latent (H₂O) and sensible heat are measured at 3.0 m with a three-axis Sonic Anemometer (CSAT3, Campbell) (Fig. 5f) pointed into the prevailing wind direction, and an

opened path infrared CO₂ and H₂O analyzer (LI7500, LI-COR) (Fig. 5f). These signals are logged to a data logger (CR5000, Campbell) at 10 Hz. It is important to estimate the turbulent fluxes between the surface and the atmosphere to understand the mechanism of the water and energy cycles over the semi-arid region of the Loess Plateau. All the necessary procedures for corrections and quality control of the turbulent fluxes are applied during post-field data processing, such as coordinating the rotation after the planar fits (PF) (Wilczak et al., 2001), frequency response corrections (Moore, 1986; Massman, 2000, 2001), sonic temperature correction (Schotanus et al., 1983), WPL correction (Webb et al., 1980), and quality control after Foken et al. (2004).

4.3.2 Large Aperture Scintillometer (LAS)

The observations of the surface sensible heat flux, representative of areas of several square kilometers, have been regularly performed with a Large Aperture Scintillometer (LAS, Kipp & Zonen) (Fig. 5g) at SACOL. This measurement is suitable for use in the energy balance and water cycle study, air pollution and regional weather forecasting, and for inertial sub-range scale turbulence measurements. Compared to the traditional “point” measurements, LAS measured larger-scale (horizontal length 0.25–4.5 km, close to the satellite pixel scale) sensible heat fluxes; it is also suitable for the validation of the study of satellite/aircraft remote sensing.

4.4 Soil and vegetation parameters monitoring system

4.4.1 Soil heat fluxes, moisture and temperature measurements

To complete the surface energy balance, soil heat fluxes (HFP01SC-L, Hukseflux) are measured at 5 and 10 cm depth. Soil moisture is measured with a water content reflectometer (CS616-L, Campbell) at 5, 10, 20, 40 and 80 cm depths; and soil temperature with a soil temperature profile (STP01-L, Hukseflux) sensor at 2, 5, 10, 20 and 50 cm depths (see Fig. 5h).

4.4.2 Soil chemical, physical and biological parameters measurement

To better understand the carbon exchange in the atmosphere-vegetation-soil system under different

land use regimes and the dynamics of soil moisture, five experimental sites have been set for measuring soil and vegetation parameters. The sites include two grasslands (fenced grassland and grazing grassland) and three croplands. Each site is 1 m² and each is adjacent to one another. When the fenced grassland was fenced in October 2005, both grasslands had been restored from cropping for 20 years and the dominant grass at the site was *Stipa. bungeana*. Three croplands were cropped with *Solanum tuberosum L.*, *Setaria italica Beauv.*, and *Semen Sesami Nigrum* in rotation, and in fallow every two or three years (See Table 3). Soil samples are taken to 100 cm at seven depths (0–10, 10–20, 20–30, 30–40, 40–60, 60–80 and 80–100 cm) and the following parameters are measured:

- Chemical parameters: SOC (soil organic carbon) is measured by using the oil bath—K₂CrO₇ titration method after digestion, and total nitrogen (Kjeldahl method) and pH[1:1(w/w) distilled water] are also measured (Chinese Editorial Committee of Soil Analysis, 1996).
- Physical parameters: Soil particle size is measured using the Automatic Granularity Laser (MALVERN, Germany) while soil bulk density measurement is carried out with the soil core method (Chinese Editorial Committee of Soil Analysis, 1996). A time-domain reflectometer (TDR) is used to monitor the dynamics of the moisture in soil.
- Biological parameters: Soil respiration is monitored with the LI-COR 6400-9 (LI-COR, Lincoln, Neb., USA; Janssens et al., 2000) while temperature and soil moisture are measured simultaneously to find out the relationship between soil respiration and these factors. To monitor the soil moisture and soil respiration dynamics, both parameters are measured once a month.

4.4.3 Vegetation parameters measurements

Quadrants are set for the measurement of vegetation parameters over the 5 sites mentioned above. Within each quadrant, all species are identified and counted and the heights of plant and vegetation cover are measured. Above-ground biomass measurement is taken with the harvest method (Ren, 1998). In the grassland, the below-ground biomass (0–100 cm)

Table 3. The rotation pattern in past four years.

	2003	2004	2005	2006
Cropland I	fallow	millet	fallow	potato
Cropland II	sesame	pea	fallow	pea
Cropland III	fallow	sesame	millet	fallow

is measured by hand washing after the soil cores are taken with an auger (9.3 cm diameter) (Ren, 1998), while in croplands, it is measured with the harvest method. Carbon and Nitrogen content in plant components are measured using the Thermo CHNS-O analyzer (Flash EA 1112). The heat value of the plant samples is measured with a Micro-computer calorimeter (WGR-1).

4.5 *Ambient air quality monitoring system*

SACOL is equipped with the ML9800 (See Fig. 5i) ambient air analyzers (Monitor Labs) which measure the concentrations of carbon monoxide (CO) (ML9830B), ozone (O₃) (ML9810B), sulfur dioxide (SO₂) (ML9850B), and oxides of nitrogen (NO/NO₂/NO_x) (ML9841B), present in the atmosphere. SACOL is also equipped with instruments that allow scientists to study the properties of tiny atmospheric particles called particulate matter (PM) and that of non-methane hydrocarbons (NMHC) which effects photochemical reactions in the troposphere. The concentration of PM₁₀ present in the boundary layer is monitored with a Beta Gauge Particulate Monitor (F-701, Durag-Verewa) (see Fig. 5j), and that of NMHC with a Total Non Methane Hydrocarbons Analyzer (TNMH 462, DANI) (See Fig. 5k).

4.6 *Aerosol optical properties monitoring system*

4.6.1 *Column aerosol optical depth*

The observations of aerosol optical depth (AOD) are made using an automatic sun tracking photometer (CE318N-VPS8, Cimel) (Fig. 5l) with 8 filters in the visible and near infrared at wavelengths of 440, 670, 870, 870, 870, 936 and 1020 nm. The sun-photometer works by measuring the intensity of the surface-reaching solar radiation at the specified wavelength bands and then converting it to optical depth by knowing the corresponding intensities at the top of the atmosphere (TOA). The TOA intensity values are periodically obtained using the Langley plot calibration technique. SACOL also has a CE318N-EBS9 with 9 measurement channels at 340, 380, 440, 500, 675, 870, 936, 1020 and 1610 nm. The instrument calibration is carried out once per year.

4.6.2 *Aerosol vertical distribution*

Aerosol vertical distribution (extinction coefficient) is measured using a Micro-Pulse Lidar system (MPL-4, Sigma Space) (Fig. 5m). The MPL has one measurement channel that records backscatter signals up to 20+ km. The primary quantity from this signal is the lowest detected cloud base in meters. Additional quan-

ties, possible through post-processing of the raw signal return, include a relative backscatter profile at 527 nm. From the relative backscatter profile other data products are possible including multiple cloud decks, cloud and layer boundaries, as well as aerosol extinction and backscatter profiles. After the new units are deployed cloud phase information will also be available.

Aerosol vertical distribution is also measured by a CAML™ Micro Lidar (CE 370-2, CIMEL & CNRS) (Fig. 5n). It is a portable, eye safe, and unattended backscattering lidar that features the ability to profile atmospheric cloud and aerosol structures and to retrieve aerosol optical and dynamic properties.

4.6.3 *Aerosol size distribution*

Aerodynamic diameter as well as the relative light-scattering intensity of aerosol particles, which are between 0.5 and 20 μm in diameter, are measured using an Aerodynamic Particle Sizer (APS-3321, TSI) (Fig. 5o), which uses a sophisticated time-of flight technique. The APS also measures the light-scattering intensity in the equivalent optical size range of 0.37 to 20 μm using a light-scattering technique. By providing paired data for each particle, the information of the make-up of an aerosol may be derived.

4.6.4 *Aerosol scattering coefficient*

The observations of the aerosol scattering coefficient are performed using a TSI Integrating Nephelometer (Model 3563) (Fig. 5p) and three ECOTECH Integrating Nephelometers (M9003). The TSI Integrating Nephelometer has three wavelengths (450, 550 and 700 nm) (Fig. 5q), and the ECOTECH Integrating Nephelometer has only one wavelength (450, 550 or 700 nm). These two kinds of nephelometers share the same principle. They are all designed specifically for studies of direct radiative forcing of the Earth's climate by aerosol particles or studies of ground-based or airborne atmospheric visual air quality.

4.6.5 *Aerosol absorption coefficient*

The aerosol light-absorption coefficient is measured at seven different wavelengths (370, 470, 520, 590, 660, 880 and 950 nm) by an aethalometer (model AE-31, Magee Sci.) (Fig. 5r), which measures the attenuation of the light beam transmitted through the aerosols deposited continuously on a quartz fiber filter paper. The difference in light transmission through the particle laden sample spot and a particle-free reference spot of the filter is used to compute the absorption coefficient. The primary propose of this instrument is to measure the aerosol black carbon (BC) concentration in the atmosphere.

4.7 Temperature and water vapor profiles

The continuous measurements of temperature and water vapor profiles are carried out with a Radiometrics Profiling Radiometer (TP/WVP-3000, Radiometrics) (Fig. 5s), which produces vertical profiles from the surface to 10 km in height by observing 5 frequency channels from 22 to 30 GHz and 7 channels from 51 to 59 GHz. The TP/WVP-3000 also produces low-resolution liquid water profiles and cloud base temperatures using a zenith-pointed infrared thermometer (IRT).

4.8 Sky conditions measurements

The observations of daytime sky conditions are performed using a TSI total sky imager (Model 880) (Fig. 5t), which is an automatic, full-color sky imaging system that provides real-time processing and display of daytime sky conditions. An onboard processor computes both fractional cloud cover and sunshine duration, storing the results and presenting data to users via an easy-to-use web browser interface. It captures images into standard JPEG files that are analyzed into fractional cloud cover.

5. Observation results

A brief summary of the key measurements obtained at SACOL from May 2006 through May 2008 is presented in this section. A more complete description of the measurements will be presented in other papers.

Figure 6 depicts the interannual variation of monthly mean downward and upward longwave (LW) radiation, downward and upward shortwave (SW) radiation, and net radiation for the period of May 2006 to May 2008. The upward longwave and downward shortwave radiation have the strongest seasonal and interannual variability, especially for summer time. Figure 7 shows the diurnal cycle and the variability of downward and upward short wave and long wave fluxes, respectively. The distribution shape of the downward and upward short wave fluxes are symmetric with a maximum at 1300 LST (Fig. 7a). The upward LW flux shows a similar pattern to the downward SW flux and follows the expected warming and cooling of surface temperatures. However, the large variability of the downward SW and upward LW fluxes are likely associated with the variability of clouds and aerosols. Figure 8 shows the diurnal cycle of net radiation for four seasons from May 2006 to May 2008. The largest net radiation occurs at noon during the summer and spring seasons, which are 35% and 100% larger than the autumn and winter seasons, respectively.

Figure 9 shows the comparison of the MODIS/CERES retrieved short wave radiative properties with

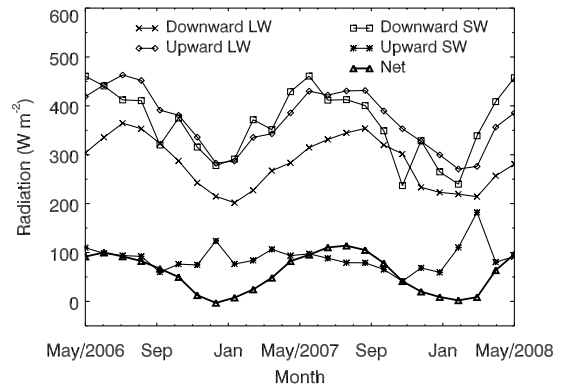


Fig. 6. Interannual variations of monthly mean downward and upward longwave (LW) radiations, downward and upward shortwave (SW) radiations, and net radiation for the period of May 2006 to May 2008.

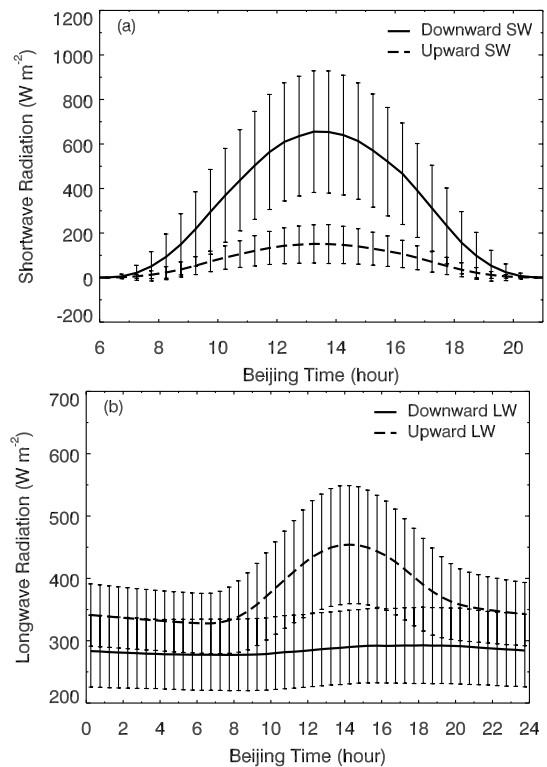


Fig. 7. Diurnal cycle and standard deviation of (a) upward and downward shortwave (SW) radiation, and (b) upward and downward longwave (LW) radiation for the period of May 2006 to May 2008.

SACOL's ground-base observations. The MODIS/CERES radiative data are from CERES SSF MODIS Edition 1B data on board Aqua. The most recent Single Scanner Footprint (SSF) dataset combines the radiation budget data from CERES with cloud property retrievals from an imager on the same platform to provide a vastly improved characterization of the in-

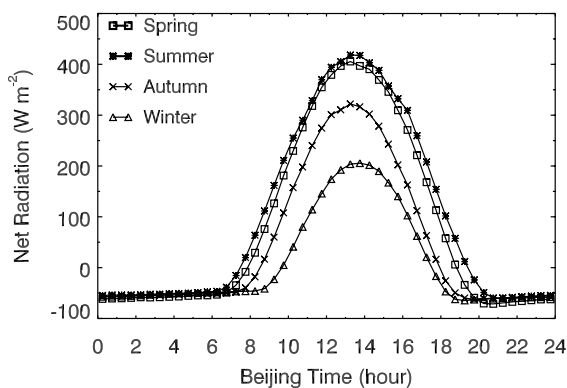


Fig. 8. Diurnal cycle of seasonal mean net radiation for period the of May 2006 to May 2008.

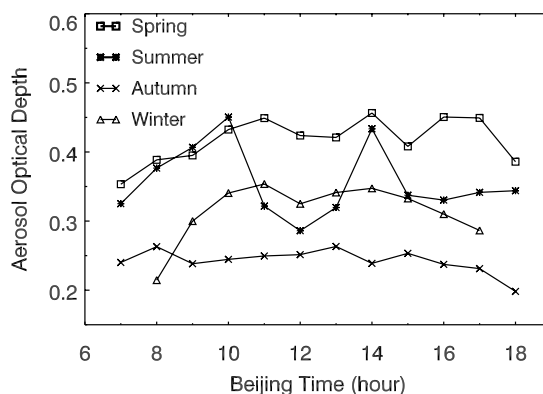


Fig. 10. Diurnal cycle of seasonal mean aerosol optical thickness for the period of May 2006 to May 2008.

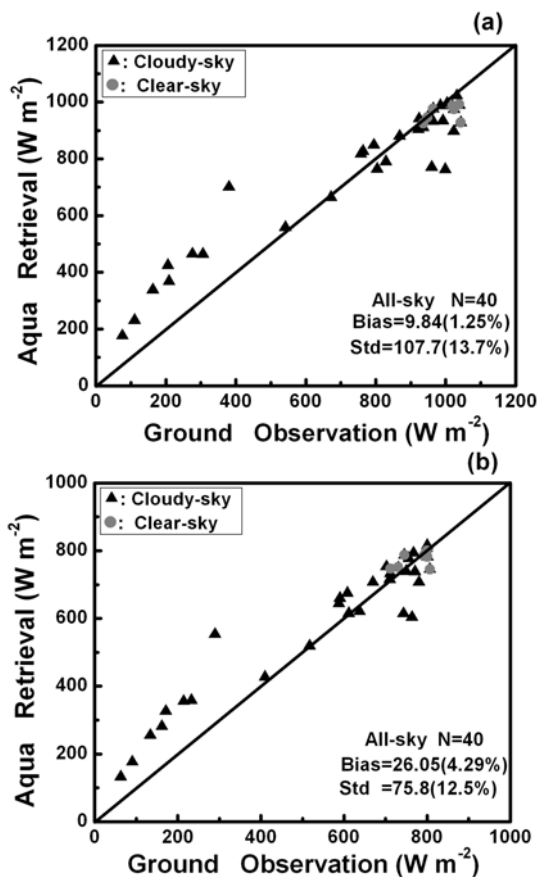


Fig. 9. Comparisons of MODIS Aqua retrieved (a) downward and (b) net shortwave radiative properties with ground-based observations.

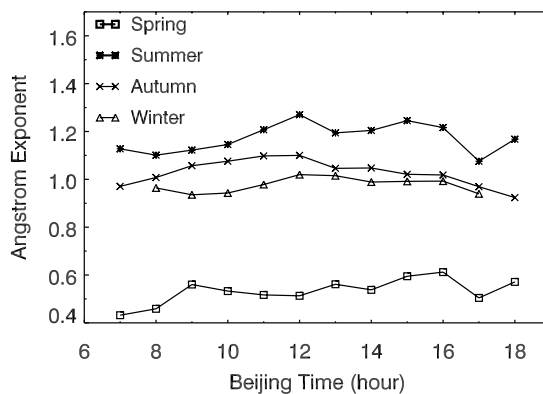


Fig. 11. Diurnal cycle of seasonal mean Angstrom Exponents for the period of May 2006 to May 2008.

stantaneous state of the atmosphere (Chambers et al., 2002). The satellite-based downward and net SW fluxes overestimate the instruments by an average of 9.84 W m^{-2} (or 1.25%) and 26.05 W m^{-2} (or 4.29%). Because the downward flux depends primarily on the

atmospheric gas and aerosol profiles and less on the surface albedo or satellite calibration, the bias of downward SW flux is smaller than the net SW flux. The reason for the larger bias of net SW flux may be due to the occurrence of convective clouds with a variety of vertical structures that cause a deviation from the plane-parallel radiative transfer assumed in the parameterization. On the other hand, the CERES narrowband-broadband calibration may not be optimal for this area.

The diurnal cycles of seasonal mean AOD at 550 nm are presented in Fig. 10, which are observed by using a Sun-Photometer (CE-318) at SACOL for a period of one year from August 2006 to July 2007. The annual averaged AOD is 0.33 and seasonal means are 0.418, 0.356, 0.315, 0.242 for spring, summer, autumn and winter, respectively. The largest averaged values of AOD are found in spring season due to the dust weather events. The diurnal cycle shows a gradual increase in the morning, reaching the maximum around 1100 LST, and then begins to decrease later in the af-

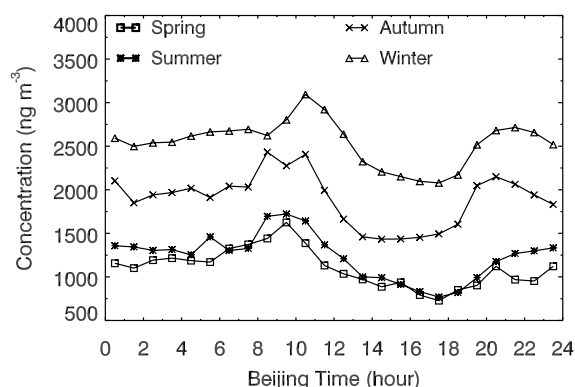


Fig. 12. Diurnal cycle of seasonal mean concentration of black carbon for the period of May 2006 to May 2008.

ternoon during spring. The diurnal variation of the winter season is similar to the spring. However, there are two strong AOD peaks in summer, the first one appears at about 1000 LST (Beijing Time) and the second comes around 1400 LST. The variability of AOD is the largest in the summer. The autumn AOD is significantly lower than other seasons and both AOD averaged value and variability are the smallest in autumn.

Figure 11 shows the diurnal cycle of seasonal mean

Angstrom Exponents α at SACOL for the same period as in Fig. 10. The Angstrom Exponent α gradually digresses from summer, autumn, winter, to spring. The annual averaged Angstrom Exponent α is 0.93 and seasonal mean are 1.17, 1.03, 0.98, 0.53 for summer, autumn, winter, and spring, respectively. It suggests that the fine particles contribute a much larger aerosol fraction in summer, while the coarse particles are the main parts in spring. The mean α value of spring is 140% less than it is in summer. This difference is related to summer rainfall and spring dust weather events. In spring, the diurnal variation of α presents a stable high value during the daytime. However, there are two α peaks in the summer, one appears at 1200 LST and the other appears at 1500 LST. The variability in summer is also larger than any other season. In autumn, α increases in the morning reaching the maximum at 1200 LST, then it begins to decrease gradually. In the winter, the value of α varies between 0.9 and 1.0.

Figure 12 shows the diurnal cycles of the seasonal mean concentration of Black Carbon (BC) for four seasons at SACOL for the period of April 2007 to March 2008. The structure of BC's diurnal cycle is the significant double-peak pattern for all seasons. The double-peak appears in the morning and evening, respectively.

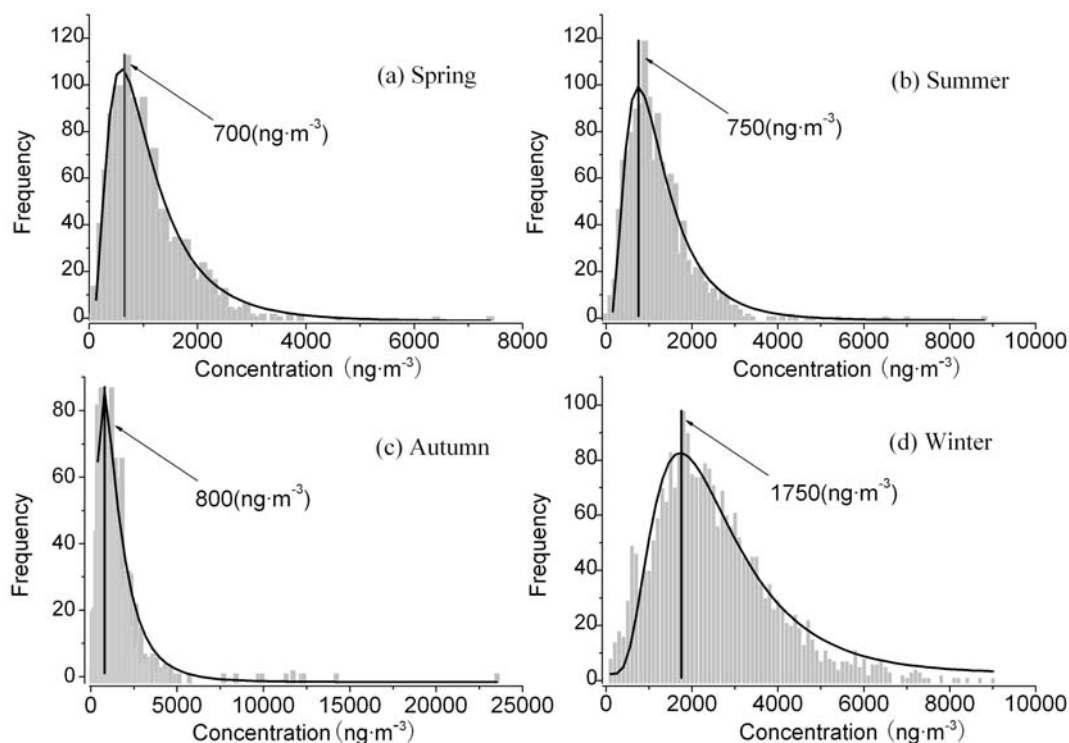


Fig. 13. Frequency distributions of hourly averaged concentration of black carbon for the four seasons for the period of May 2006 to May 2008.

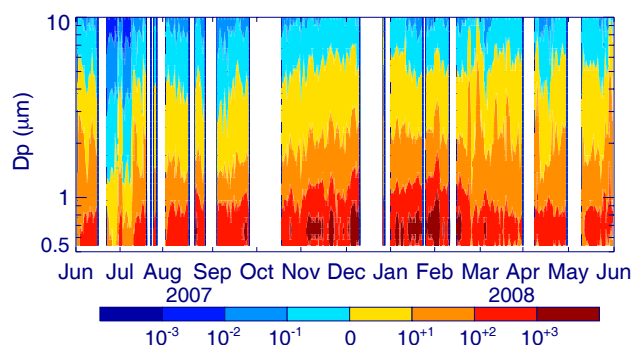


Fig. 14. Seasonal average aerosol number size distribution at SACOL as deduced from APS (Aerodynamic Particle Sizer) measurements ($0.542 \leq D_p \leq 10 \mu\text{m}$) for period of June 2007 to May 2008. D_p denotes particle diameter.

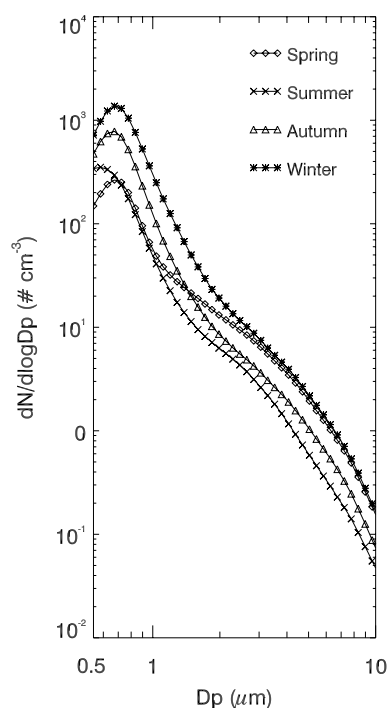


Fig. 15. Seasonal average aerosol number size distribution at SACOL as deduced from APS (Aerodynamic Particle Sizer) measurements ($0.542 \leq D_p \leq 10 \mu\text{m}$) for the period of June 2007 to May 2008. D_p denotes particle diameter, and N particle numbers.

The concentration of BC shows a gradual digression from winter, autumn, summer, to spring. The first peak of BC appears about one hour later in autumn and winter than other seasons, which may be controlled both by the characteristics of the atmosphere boundary layer and anthropogenic influences.

Figure 13 shows the frequency distributions of

hourly averaged concentration of BC for all seasons at SACOL for the period of April 2007 to March 2008. Based on log-normal statistics, the background concentration of Black Carbon in this area was estimated to be approximately 850 ng m^{-3} , which is lower than the value in Wenjiang (2850 ng m^{-3}) and higher than the results from Mt. Waliguan (65 ng m^{-3}). By using the same method, the background concentrations in different seasons are 700 ng m^{-3} (spring) (Fig. 13a), 750 ng m^{-3} (summer) (Fig. 13b), 800 ng m^{-3} (autumn) (Fig. 13c), and 1750 ng m^{-3} (winter) (Fig. 13d), respectively. It can be found that the background concentration in winter is nearly twice the other seasons, due to increased coal consumption for heating. Although it is the rainy season in this region, the summer concentration of BC is still much higher than Mt. Waliguan.

The size-separated number concentrations in the range of $0.5 \mu\text{m} \leq D_p \leq 10 \mu\text{m}$ (D_p denotes particle diameter) has been observed since June 2007 at the SACOL by using an Aerodynamic Particle Sizer (TSI APS Model 3321). The particle size measurements permit the determination of a fraction of fine mode ($0.5 \mu\text{m} \leq D_p \leq 1 \mu\text{m}$) particles and coarse mode ($1 \mu\text{m} \leq D_p \leq 20 \mu\text{m}$) particles with a 5-minute time resolution. The instrument is based on the quantification of the 90° scattering of light by aerosol particles. Figure 14 shows the daily averaged aerosol number size distribution for the period of June 2007 to May 2008. The reasons for dismissing data were due to instrument failures or rainy conditions. The averaged diurnal size distributions is 921.46 m^{-3} (winter), 178.26 m^{-3} (spring), 222.05 m^{-3} (summer) and 509.39 m^{-3} (autumn) for fine mode particle ($0.5 \mu\text{m} \leq D_p \leq 1 \mu\text{m}$) and 30.34 m^{-3} (winter), 10.28 m^{-3} (spring), 6.32 m^{-3} (summer) and 12.36 m^{-3} (autumn) for coarse mode particle ($1 \mu\text{m} \leq D_p \leq 10 \mu\text{m}$), respectively.

The APS continuous measurement conducted at SACOL also permits the ability to obtain information concerning the seasonal averaged size distribution for the fine mode and coarse mode. The seasonal averaged size distributions for the period of June 2007 to May 2008 are shown in Fig. 15, which are characterized by the highest number concentration in winter and the lowest in summer, with a typical shape of background areas. The number concentration relative maximum was evident at the $D_p \sim 0.7 \mu\text{m}$ (5th APS channel), indicating the possible shifting between fine and coarse mode. This high value of particles in winter may be related the biomass burning, which can produce large amounts of fine mode particle. The aerosol size number concentration in spring is relatively lower than the other seasons for the coarse mode particle at SACOL.

Figure 16 shows the diurnal cycle of surface latent

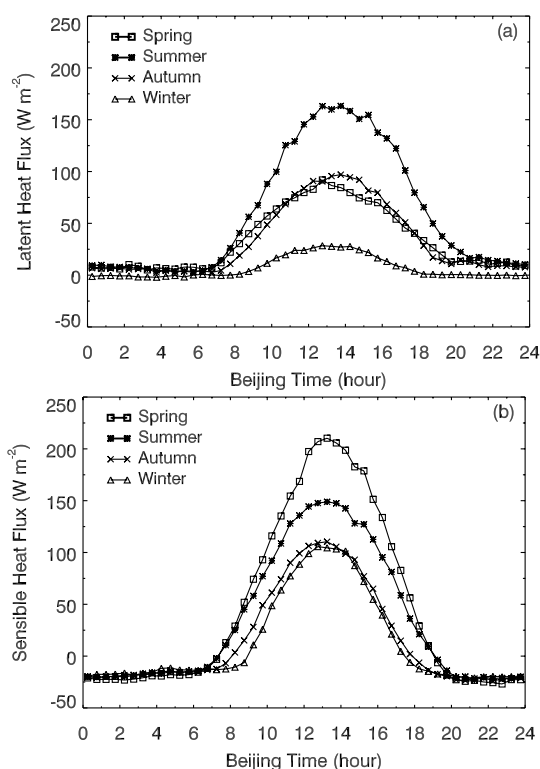


Fig. 16. Diurnal cycle of seasonal mean surface fluxes for (a) latent heat and (b) sensible heat fluxes for the period of May 2006 to May 2008.

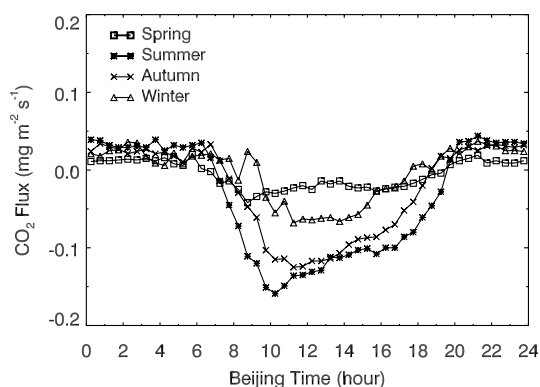


Fig. 17. Diurnal cycle of seasonal mean CO_2 flux for the period of May 2006 to May 2008.

heat and sensible heat flux at SACOL. In general, it shows that latent heat flux is high with a maximum around noon (1100 LST to 1600 LST) for summer (Fig. 16a). The averaged sensible heat flux is positive during the daytime, i.e. sensible heat flux is transported away from the surface (Fig. 16b). However, there is negative sensible heat flux at during the nighttime (Fig. 16b).

Figure 17 displays the diurnal cycle of seasonal mean CO_2 uptake at SACOL for the four seasons. The CO_2 fluxes in Fig. 17 are normalized by the average of each 30 min. The processing procedures applied to CO_2 dataset are the same as latent and sensible heat flux, except the air density fluctuation effect correction which is not applied to CO_2 . In winter and spring, the CO_2 fluxes are less than $0.05 mg m^{-2} s^{-1}$ (in the figures a negative value indicates a net flux into the vegetation, i.e., a sink) and there are no obvious diurnal variations due to the bare surface and weak terrestrial carbon exchange. In summer and autumn, the CO_2 fluxes shows significant diurnal variability with a negative maximum at 1000 LST and positive values during the nighttime.

Figure 18 shows the temperature, relative humidity and liquid water contours to 10 km height retrieved from a radiometric profiler with rain effect mitigation. Surface temperature, relative humidity, pressure, cloud base temperature, rain flag, and column integrated vapor and liquid are shown (counterclockwise) in the 24-h time series plots. Figure 19 shows normalized relative backscatter intensity as functions of local time and altitude collected by the SACOL MPL on 26 June 2007. The aerosol back scatter was observed between 1 and 3 km with a cloud layer from 5 to 8 km during night and early morning, and this aerosol layer persisted the whole day. A mixed aerosol-cloud layer between 3 and 5 km was also observed during the morning hours. Figures 18 and 19 suggest that the microwave radiometer and lidar are useful in determining the vertical structure of cloud and aerosol layers.

6. Concluding remarks

The observational facilities of SACOL represent a unique resource for climate research and should allow the community to focus its effort on the high priority problem of understanding semi-arid climates. SACOL employs a multiplatform approach, with state-of-the-art instrumentation deployed at the surface to provide a comprehensive description of atmosphere and land surface thermodynamic state, particulate composition, aerosol, cloud and radiative properties. This integrated dataset is being used to improve the understanding of aerosol-climate interaction, and to test and improve climate model and satellite remote sensing techniques. Results of the analyses performed to date have been summarized in this paper and are reported in more detail elsewhere in other papers. SACOL's rich data can be accessed online through the SACOL home page at <http://climate.lzu.edu.cn>.

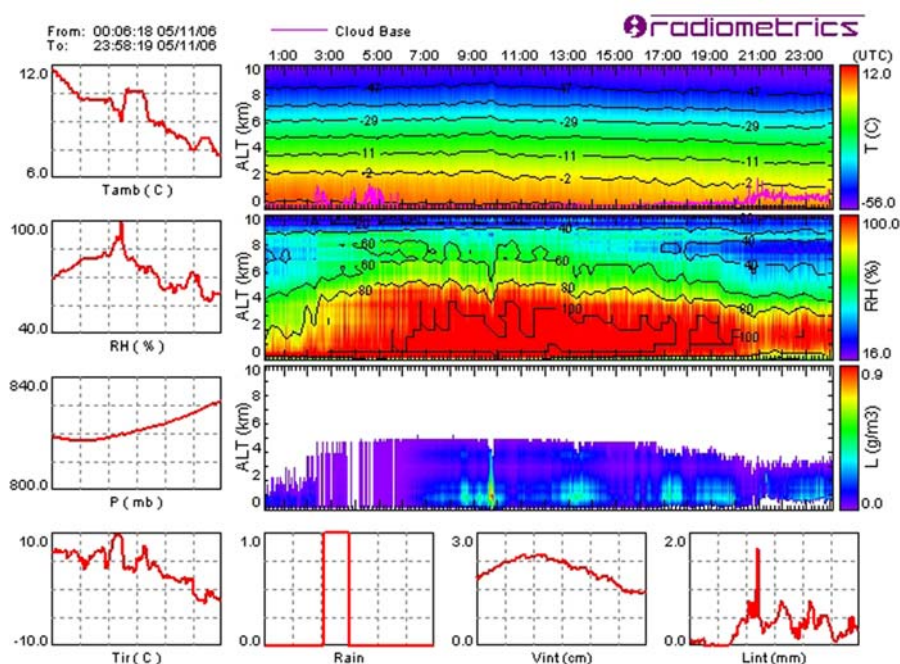


Fig. 18. Temperature, relative humidity and liquid water contours to 10 km height retrieved from a radiometric profiler with rain effect mitigation. Surface temperature, relative humidity, and pressure, cloud base temperature, rain flag, and column integrated vapor and liquid are shown (counterclockwise) in the 24-h time series plots.

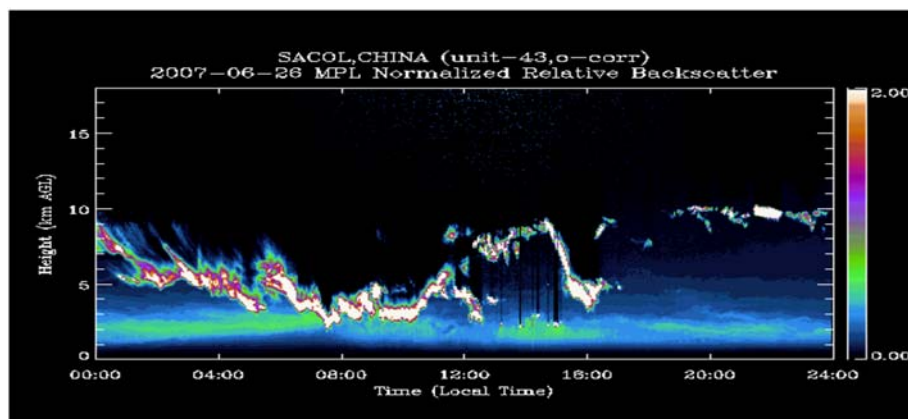


Fig. 19. Micro-Pulse Lidar normalized relative backscatter intensity for 26 June 2007.

Acknowledgements. SACOL was sponsored by Lanzhou University through 985 Program; the National Basic Research Program of China under Grant No. 2006CB400501, and the National Natural Science Foundation of China under Grant Nos. 40633017 and 40725015. We are grateful for the excellent support provided by the people at the College of Atmospheric Sciences, Lanzhou University. We also thank, Drs. Daren Lü, Jianmin Xu, Ronghui Huang, Guoxiong Wu, Si-Chee Tsay, Zhanqing Li, Qiang Fu, Qilong Min, and Qiang Ji, for their useful suggestions.

REFERENCES

Alexandrov, M. D., A. A. Lacis, B. E. Carlson, and B. Cairns, 1999: Remote sensing of atmospheric aerosols, nitrogen dioxide, and ozone by means of multi-filter rotating shadow-band radiometer. *Remote Sensing of Clouds and Atmosphere*, J. Russell, and C. Serio, Eds., Proc. SPIE 3867, 156–170.

Bao, Y., and S. Lu, 2006: Review of land-atmosphere interaction research in Arid and Semi-arid regions. *Journal of Desert Research*, **3**, 134–140. (in Chinese)

Breon, F.-M., D. Tanre, and S. Generoso, 2002: Aerosol

- effect on cloud droplet size monitored from satellite. *Science*, **295**, 834–838.
- Chambers, L. H., B. Lin, and D. F. Young, 2002: Examination of new CERES data for evidence of tropical iris feedback. *J. Climate*, **15**, 3719–3726.
- Chinese Editorial Committee of Soil Analysis, 1996: *Soil Physical and Chemical Analysis and Description of Soil Profile*. China State Standards Press, 266pp. (in Chinese)
- Crowley, T. J., 2000: Causes of climate change over the past 1000 years. *Science*, **289**, 270–277.
- DeMott, P. J., K. Sassen, M. Poellot, D. Baumgardner, D. C. Rogers, S. Brooks, A. J. Prenni, and S. M. Kreidenweis, 2003: African dust aerosols as atmospheric ice nuclei. *Geophys. Res. Lett.*, **30**, 1732, doi:10.1029/2003GL017410.
- Foken, T., M. Göckede, M. Mauder, L. Mahrt, B. D. Amiro, and J. W. Munger, 2004: Post-field data quality control. *Handbook of Micrometeorology: A Guide for Surface Flux Measurements*, Lee et al., Eds., Kluwer, 181–208.
- Harrison, L., and J. Michalsky, 1994: Objective algorithms for the retrieval of optical depths from ground-based measurements. *Appl. Opt.*, **33**, 5126–5132.
- Harrison, L., J. Michalsky, and J. Berndt, 1994: Automated multifilter rotating shadow-band radiometer: An instrument for optical depth and radiation measurements. *Appl. Opt.*, **33**, 5118–5125.
- Holben, B. N., and Coauthors, 1998: AERONET—A federated instrument network and data archive for aerosol characterization. *Remote Sens. Environ.*, **66**, 1–16.
- Houghton, J. T., Y. Ding, D. J. Griggs, M. Noguer, P. J. van der Linden, and D. Xiaosu, 2001: *Climate Change 2001: The Scientific Basis*. Cambridge University Press, 944pp.
- Hu, Y., 1994: Research advance about the energy budget and transportation of water vapor in the HEIFE area. *Advance in Earth Sciences*, **9**, 30–34. (in Chinese)
- Hu, Y., and Y. Gao, 1994: Some new understandings of processes at the land surface in arid area from the HEIFE. *Acta Meteorologica Sinica*, **52**, 285–296. (in Chinese)
- Huang, J. P., B. Lin, P. Minnis, T. Wang, X. Wang, Y. Hu, Y. Yi, and J. R. Ayers, 2006a: Satellite-based assessment of possible dust aerosols semi-direct effect on cloud water path over East Asia. *Geophys. Res. Lett.*, **33**, doi: 10.1029/2006GL026561.
- Huang, J. P., P. Minnis, B. Lin, T. Wang, Y. Yi, Y. Hu, S. Sun-Mack, and K. Ayers, 2006b: Possible influences of Asian dust aerosols on cloud properties and radiative forcing observed from MODIS and CERES. *Geophys. Res. Lett.*, **33**, L06824, doi: 10.1029/2005GL024724.
- Huang, R., 2004: Advances of the project of the formation mechanism and p theory of severe climatic disasters in China. *China Basic Science*, **4**, 6–16. (in Chinese)
- Iwasaka, Y., and Coauthors, 2003: Nature of atmospheric aerosols over the desert areas in the Asian continent: chemical state and number concentration of particles measured at DunHuang, China. *Water, Air, and Soil Pollution: Focus*, **3**, 129–145.
- Iwasaka, Y., and Coauthors, 2004: Pool of the dust particles over the Asian continent, balloon-borne optical particle counter and ground-based lidar measurements at Dunhuang, China. *Environmental Monitoring and Assessment*, **92**, 5–24.
- Janssens, I. A., A. S. Kowalski, B. Longdoz, and R. Ceulemans, 2000: Assessing forest soil CO₂ efflux: An in situ comparison of four techniques. *Tree Physiology*, **20**, 23–32.
- Kawamoto, K., and T. Nakajima, 2003: Seasonal variation of cloud particle size from AVHRR remote sensing. *Geophys. Res. Lett.*, **30**, 1810–1813.
- Liu, H., W. Dong, C. Fu, and L. Shi, 2004: The long-term field experiment on aridification and the ordered human activity in semi-arid area at Tongyu, Northeast China. *Climatic and Environmental Research*, **9**, 352–378. (in Chinese)
- Lu, D., and Coauthors, 2002: Composite study on Inner Mongolia semiarid grassland soil-vegetation-atmosphere interaction (IMGRASS). *Earth Science Frontiers*, **9**, 52–63. (in Chinese)
- Lu, D., Z. Chen, J. Chen, G. Wang, J. Ji, H. Chen, and Z. Liu, 2005: Study on soil-vegetation-atmosphere interaction in Inner Mongolia semiarid grassland. *Acta Meteorologica Sinica*, **63**, 33–55. (in Chinese)
- Mann, M. E., R. S. Bradley, and M. K. Hughes, 1999: Northern hemisphere temperatures during the past millennium: inferences, uncertainties, and limitations. *Geophys. Res. Lett.*, **26**, 759–762.
- Massman, W. J., 2000: A simple method for estimating frequency response corrections for eddy covariance systems. *Agricultural Forest Meteorology*, **104**, 185–198.
- Massman, W. J., 2001: Reply to comment by Rannik on “A simple method for estimating frequency response corrections for eddy covariance systems”. *Agricultural Forest Meteorology*, **107**, 247–251.
- Min, Q. 1996: Cloud properties derived from surface MFRSR measurements and comparison with GOES results at the ARM SGP site. *Geophys. Res. Lett.*, **23**, 1641–1644.
- Moore, C. J., 1986: Frequency response corrections for eddy correlation systems. *Bound.-Layer Meteorol.*, **37**, 17–36.
- Ramanathan, V., P. J. Crutzen, J. T. Kiehl, and D. Rosenfeld, 2001: Aerosols, climate, and the hydrological cycle. *Science*, **294**, 2119–2124.
- Ren, J. Z., 1998: *Research Method of Prataculturae Science*. Chinese Agriculture Press, 441pp. (in Chinese)
- Rosenfeld, D., Y. Rudich, and R. Lahav, 2001: Desert dust suppressing precipitation: A possible desertification feedback loop. *Proceedings of the National Academy of Sciences*, **98**, 5975–5980.
- Schotanus, P., F. T. M. Nieuwstadt, and H. A. R. De-

- Bruin, 1983: Temperature measurement with a sonic anemometer and its application to heat and moisture fluctuations. *Bound.-Layer Meteor.*, **26**, 81–93.
- Twomey, S., 1977: Influence of pollution on shortwave albedo of clouds. *J. Atmos. Sci.*, **34**, 1149–1152.
- Webb, E. K., Pearman, G. I., and R. Leuning, 1980: Correction of flux measurements for density effects due to heat and water vapour transfer. *Quart. J. Roy. Meteor. Soc.*, **106**, 85–100.
- Welton, E. J., J. R. Campbell, J. D. Spinhirne, and V. S. Scott, 2001: Global monitoring of clouds and aerosols using a network of micropulse lidar systems. Vol. 4153, *Proc. Lidar Remote Sensing for Industry and Environmental Monitoring*, Sendai, Japan, SPIE, 151–158.
- Wilczak, J. M., S. P. Oncley, and S. A. Stage, 2001: Sonic anemometer tilt correction algorithms. *Bound.-Layer Meteor.*, **99**, 127–150.
- Zhang, H. S., J. Y. Chen, and S.-U. Park, 2001: Turbulence structure in the unstable condition over various surfaces. *Bound.-Layer Meteor.*, **100**, 243–261.
- Zhang, Q., and Coauthors, 2005: NWC-ALIEX and its advances. *Advance in Earth Sciences*, **20**, 60–74. (in Chinese)